Description of Position Control Laws for Functionality Test of a Bi-modal Morphing Flap

M. C. Noviello
Department of Industrial Engineering- Aerospace Division, University of Naples "Federico II", Naples, Italy
Email: mariachiara.noviello@unina.it

F. Rea, M. Arena, R. Pecora and F. Amoroso
Department of Industrial Engineering- Aerospace Division, University of Naples "Federico II", Naples, Italy
Email: {francesco.rea, maurizio.arena, rosario.pecora, f.amoroso}@unina.it

***Abstract*— Modern aerospace research programs are increasingly focusing on structural design strategies based on the adaptive wing philosophy. Morphing wing technologies are being studied because they can be used to maximize the aerodynamic efficiency, maneuverability, and load control effectiveness under different flight conditions. As one of the most important research projects in Europe, the JTI Green Regional Aircraft (GRA) focused on the design and demonstration of a true-scale morphing flap applicable to the natural laminar flow (NLF) wing of a 130-seat EASA CS25 category reference aircraft. The authors worked on developing an appropriate actuation and control system to enable flap bi-modal operational modes. In the deployed configuration, the overall camber morphs during take-off and landing for high-lift performances. In the stowed configuration, the flap trailing edge (nearly 10% of the local chord) is deflected upwards and downwards to improve the wing aerodynamic efficiency during cruising. Tailored control units were programmed according to a proper digital logic control law based on LTI DriveManager® software. Flap functionality tests showed that the obtained morphed shapes had an excellent correlation with the design target geometries.**

***Index Terms*—morphing flap prototype, digital logic law, plugs programming, functionality test.**

I. Introduction

Morphing is a bio-inspired concept; the critical and meticulous observation of the elegance of birds' flight has always inspired man [1]. This has led aerospace engineers to focus on metamorphic, or adaptive, wing structures capable of adapting their shape in a continuous manner for the entire flight envelope [2]. Morphing structures can potentially deliver several operational benefits, such as reducing drag and thus increasing range and fuel efficiency [3], optimal load control, and augmenting the effectiveness of control surfaces [4].

In this context, the European research project of Clean Sky Green Regional Aircraft (GRA) sought to join different morphing concepts for application to large civil aircraft. In the low noise configuration domain of the Clean Sky program, an advanced high lift system has been designed and validated for the natural laminar flow wing of the next-generation GRA (130 seats, open rotor configuration). In detail, a true-scale segment of the outer wing flap region was selected as the investigation domain (Fig. 1): spanning 3.6 m from the wing kink with a root chord equal to 1.2 m and taper ratio equal to 0.75. The bi-modal morphing capabilities were investigated to increase the aircraft performances during all flight phases (take-off, climbing, cruising, descent, and landing) and thus reduce the fuel consumption per mission.

In accordance with project requirements [5], target morphed shapes were defined to enable two operational modes:

1. Overall camber morphing (flap deployed) to improve the high-lift performances during take-off and landing;
2. Tab-like deflection (flap stowed), where the device tip rotates by the angle β in the range [−10°, +10°] (Fig. 2) for load control during climbing, cruising, and descent.

A novel rib kinematic mechanism was properly designed and moved by eight servo-actuators driven by specific control units, here described. This enables the transition from the baseline shape to the target flap morphed shapes (Fig. 2).

This paper presents a detailed description of the actuation and control system that allows these flap morphing capabilities and functionality tests performed for validation.

The adopted design solutions were carefully selected to assure overall device compliance with industrial standards and applicable airworthiness requirements [7].

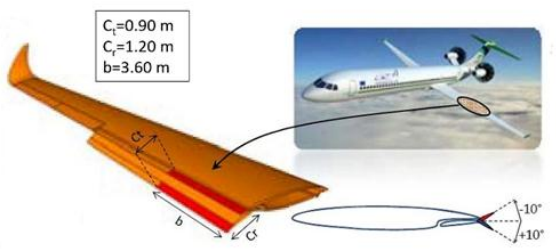

Figure 1. Bi-modal morphing flap investigation domain and tip deflections

Manuscript received March 15, 2018; revised December 10, 2018.

doi: 10.18178/ijmerr.8.1.31-40

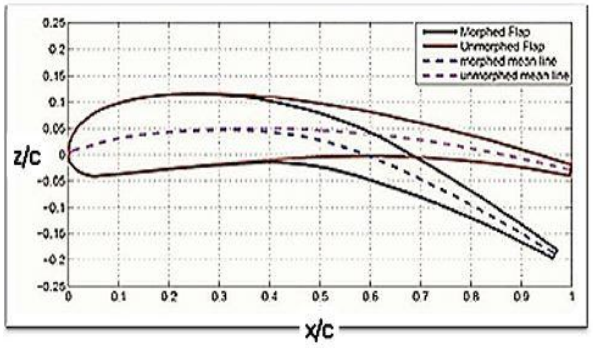

Figure 2. Baseline and morphed configurations of the flap airfoil.

II. Overview of the Morphing Flap Structure

The flap architecture is composed of eight consecutive active ribs in the span-wise direction that divide the structure into seven bays (Fig. 3). The ribs' structural layout was conceived to have a finger-like configuration to change into the target shapes (Fig. 2). Each rib (Fig. 4) is divided into four consecutive blocks (B0, B1, B2, and B3). Three frictionless hinges (A, B, C) along the camber line allow relative rotations among adjacent blocks. The rib mechanism uses a four-segment polygonal line to approximate the camber line of the flap aerofoil and morph into the target configuration while keeping the aerofoil thickness distribution unchanged.

Referring to Fig. 4, the interconnection between blocks B0 and B2 occurs by means of a suitably shaped linking beam (L), with two hinges at the extremities. The internal leverage K1 is placed into block B1 and connects blocks B1 and B3. The external rotary actuator A1 activates this leverage, which amplifies the motor torque. In such a way, the leverage K1 is induced to move and, consequently, to change the relative position of block B1 with respect to B3. At the same time, blocks B0 and B2 are constrained to move according to B1 and B3 movements, because of the mutual interconnection to them. The position of the link L and of the hinges of the leverage K1 were studied so that, under the rotation of A1 shaft, the ribs' blocks can rotate around cylindrical hinges A, B, C according to properly defined angles, compliant with the external target morphed shapes (overall camber morphing).

On the other hand, the rotation of the actuator A2 induces the secondary leverage K2 (hosted by block B2) to drive the relative rotation between B3 and B2. The secondary leverage amplifies the torque of the actuator A2, enabling B3 rotation around the hinge C thus allowing the tab-like deflection. The morphing mode 1 requires the activation of only actuator A1, while keeping fixed the secondary leverage; on the contrary, actuator A2 is the only one to be powered on during the morphing mode 2. Rotary encoders were installed on the cylindrical hinges (A, B, C) of the ribs placed at first, third and eighth rib station (from root to tip) (Fig. 3) to measure the relative rotation of the rib-blocks. Morphing ribs' layout adaptation was needed to fit the geometry of the flap at each span-wise section. For that purpose, while the chordwise length of blocks B1 and B2 was kept equal for all flap section, an extension of the chordwise length of blocks B0 and B3 was necessary to obtain hinge lines perpendicular to ribs' reference planes.

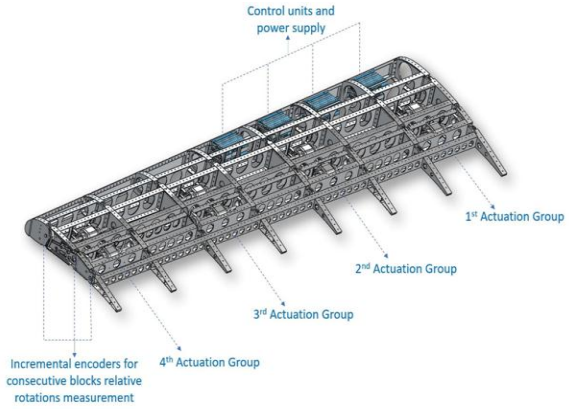

Figure 3. Bi-modal morphing flap structure and equipment.

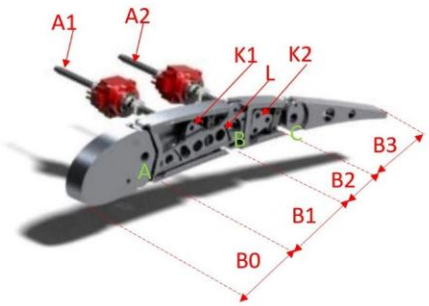

Figure 4. Morphing ribs' layout

All blocks B0 and B3 were linked along the span through two C-shaped continuous spars (Al 2024-T351), located at the 5% and 70% of the local airfoil and conceived to carry the greatest amount of external loads and adequate deformation levels.

Segmented spars (Al 2024-T351) ad stringers were properly shaped to define a multi-box structure elastically stable under torsion and bending. On both upper and lower side of ribs and longitudinal stiffening components, segment skin was installed (Fig. 5).

More in detail, four elements in Al 2024-T4 were conceived for each side of the morphing flap device to slide each other as armadillo shells. To avoid friction effects between consecutive skin segments, rubber seals were used.

Advanced kinematic analyses allowed for defining the shape of the seals by simulating flap morphing modes; these analyses also verified the implemented assembly tolerances without clashes due to consecutive subcomponents in relative motion each other.

Skin panels were obtained by sheet forming, while all the other structural metallic parts were produced by numeric-control machines.

The reversibility of the prototype's assembly process required to avoid riveting along the interface regions, preferring the implementation of screwed joints: for that

purpose, the thickness of components along the interface regions was increased with respect to the design values.

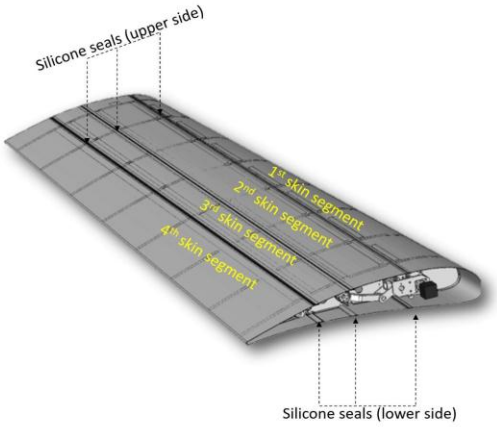

Figure 5. Morphing flap segmented skin and rubber seals.

III. Morphing Flap Actuation and Control System Design

A novel morphing architecture was developed to enable the flap sections to the transition from the un-morphed (baseline) to the target shapes, as explained in Section 2. The innovative structure was then physically combined with actuation and control systems solutions for analysis. The investigated outer flap equipment was composed of four actuation groups, eight control devices, and rotary encoders to measure the relative rotations. Fig. 6 shows the actual top views of the flap with integrated equipment omitting the skin, to focus on the internal mechanized structural arrangement, [6].

Figure 6. Morphing flap prototype sideview.

A. Actuation System Design

Adaptive lifting surfaces such as the flap can be considered as articulate systems requiring high functionality with inevitable structural design complexity [8]. More specifically, an adaptive structure allows for a controlled and fully reversible transition from the baseline shape to a variety of different configurations [9]. The choice of the actuation mechanism represents one of the most critical project phases for optimizing the structural design of the morphing flap [10]. The system must be compliant with the design requirements, so it must be compact and robust while being able to morph and preserve a given shape configuration under the action of relevant aerodynamic loads [5]. To address these issues, a new concept for the kinematic mechanism was developed to ensure bi-modal camber morphing of flap ribs [11].

The design process of the actuation system needed to activate the ribs' motion began with static analysis through finite element simulations. The highest hinge torque resistance (H_T = 150 N-m [5]) was found to correspond to the hinge linking blocks B2 and B3 (point C in Fig. 4). As a conservative approach, the whole actuation kinematic mechanism was developed by considering this hinge torque resistance as the design torque.

The high torque resistance required the actuators to be coupled with Harmonic Drive® HFUC-17-2UH devices (two for each motor shaft) acting as gear reducers and actuation torque amplifiers (Fig. 7). The amplification factor of the specific gear reducers (RHD) was 120 [5]. Table I presents the technical specifications.

TABLE I. Torque Amplifier Features [7]

Specification	*Harmonic Drive HFCU-17-2H*
Maximum torque	54 Nm
Gear ratio	120
Maximum speed	60 rpm
Moment stiffness	16×10^3 Nm/rad
Weight	0.64 Kg

The kinematic mechanism torque amplification factor (K_{ma}) had a minimum value of 5 and varied as a function of the hinge rotation angle (Fig. 8, in logarithmic scale). The actuation system layout was conceived so that the two Harmonic Drives were keyed to each motor shaft, and every individual actuator simultaneously moved two consecutive blocks [12]. Therefore, not considering friction effects, a minimum motor torque of 0.5 N-m was necessary to overcome the design hinge torque. Fig. 9 shows the complete actuation design process.

In order to consider friction effects [13], a conservative choice of motors was made by selecting KOLLMORGEN® KBM-14H01-B because of its high level of performance. Fig. 9 shows the continuous stall (dotted red curve) and peak stall torque (continue red curve) of the motors to be a function of the operating speed range. Table II presents all motor features, and Figure 10 shows the architecture.

TABLE II. Motor Performance Data [7]

Specification	*Actuator Model KBMS-14*
Continuous stall torque	1.2 Nm
Peak stall torque	3.5 Nm
Maximum speed	8000 rpm
Peak current	10 A
Weight	2.5 Kg

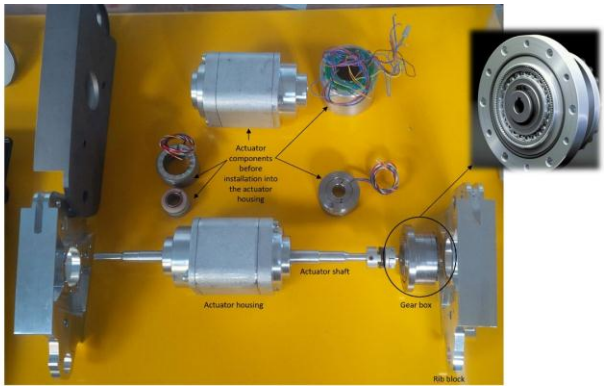

Figure 7. Actuator/rib interface and gear box zoom (on the top right corner).

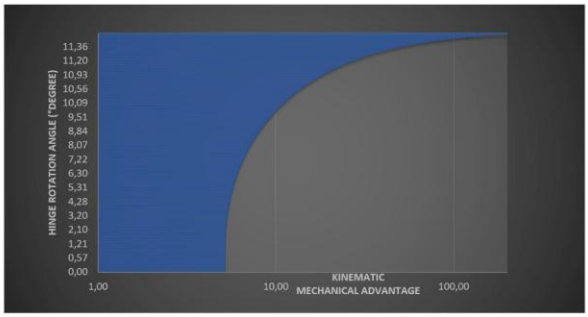

Figure 8. Kinematic mechanical advantage as a function of C hinge rotation angle (°degrees).

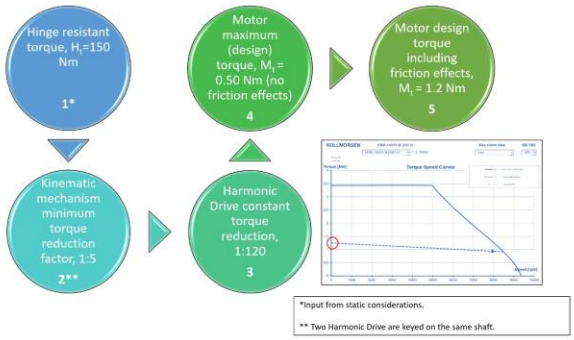

Figure 9. Actuation design procedure and KBM-14h01-B motor performance curves.

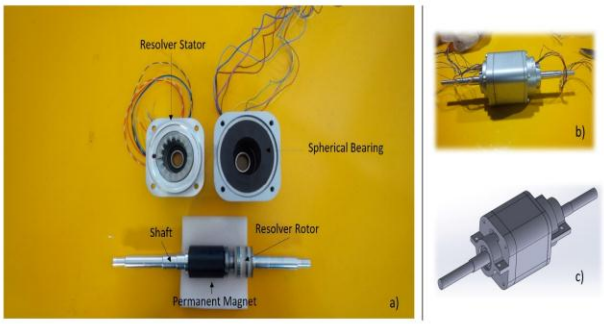

Figure 10. KBM-14h01-B motor: a) before installation; b) after installation; c) 3D CAD drawing.

For each rib kinematic mechanism, the total output torque (T_{ot}) was assessed as follows:

$$T_{ot}=M_t \times R_{HD} \times K_{ma} \times C_{fHD} \quad (1)$$

where M_t is the motor torque, which was assumed to be constant and equal to the half of the stall torque (0.6 Nm) corresponding to the operating speed (400 rpm); R_{hd} = 120 is the Harmonic Drive constant torque amplification factor; K_{ma} is the kinematic mechanical gain whose trend was previously described; and C_{fHD} represents the torque correction factor, which includes the Harmonic Drive maximum torque with respect to the product $M_t \times R_{hd}$, and thus was 0.75.

Fig. 11 presents the actuation total output torque (1) (with and without the C_{fHD} correction factor) and torque trends at hinge C in logarithmic scale as functions of the hinge rotation angle.

The actuation system was found to be very capable of overcoming the hinge torque resistance.

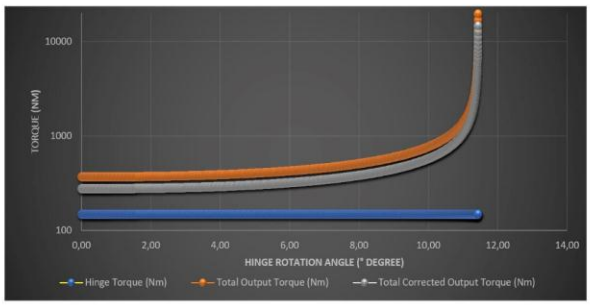

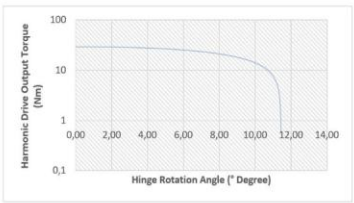

Figure 11. On the top: C hinge, total output and corrected total output torques (Nm) trend as a function of C hinge rotation angle (°degree). On down: Harmonic Drive output torque as a function of C hinge rotation angle (°degree).

B. *Control Units and Motors Installation and Configuration*

In order to activate flap bi-modal morphing capabilities [14], a proper control system was studied and developed. It consisted of:

- Eight control units (ServoOne Jr by LTI® motion, Figure 12) coupled and stacked along the first four bays of B0;
- A power supply with a main voltage of 24 V;
- Switch-LAN for correct wiring through a TCP-IP connection controller-drive.

In general, predefined movements of the motors can be achieved thanks to tailored control units (or controllers). These devices can be configured as a master or slave if they respectively provide or receive (to emulate) an electrical command pulse wave.

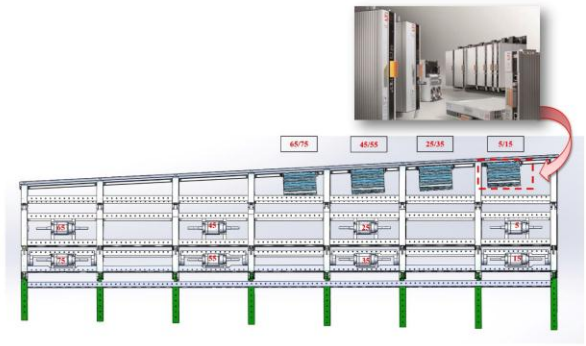

Figure 12. Bi-modal morphing flap top view: zoom on LTI ServoOne Jr® controller units (on the top right corner).

The first action needed during controllers' configuration was a correct physical installation and wiring. More in detail, to provide proof of compliance with the required protection targets, referring to Figure 13, it was considered that:

1. Each motor was connected to its own control unit corresponding to X1 terminal by using shielded cables;
2. The connection between each controller and the power supply (+24 V DC) occurred through X2 terminal by using shielded cables, stripping them back only as short as necessary before the control supply connection;
3. The wire strands at the output of the mains filter was directly connected to the AC mains (X3) of the ServoOne Junior; the voltage supply to the ServoOne Junior was separate for the control and power sections. This provided reliable protection against electric shock on the control side. The control supply was connected first, thus parameterizing the device with DriveManager® 5.5.27 and, above all, setting to the correct power supply (3 x 230 V AC, since the investigated system is three-phase, Fig. 14);
4. At the control-logic terminals (X4) of the ServoOne junior, the shielding of the control cable was stripped back only as short as necessary. The connection between each controller device was realized with a jumper cable, thus assuring correspondence between plugs and terminal pins (for the goals of this activity, not all the plugs were programmed, Fig. 13). Such a connection made it possible to synchronise the activation of the master and slave devices with a specific logic. The controllers and corresponding motors were (arbitrarily) numbered 5, 15, 25, 35, 45, 65, and 75 (Fig. 15);
5. All resolver connections occurred at X6 terminal, located on the top of control units;
6. TTL encoder connections among master and slave controllers were obtained by means of X8 plug, allowing for more controllers to work in electrical axis (one axis acted as master, and the others as slave). The master axis generates a pulse train that becomes the reference signal for the slave axes.
7. X9 terminal of each controller was connected to a switch-LAN, which cable was introduced into the PC, Fig. 15.

Controllers' simplified layout with corresponding plugs and terminals is shown in Fig. 13.

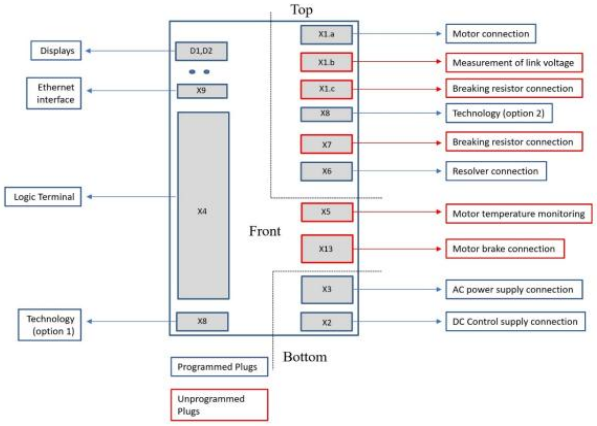

Figure 13. Controller simplified layout with programmed (blue) and unprogrammed (red) plugs.

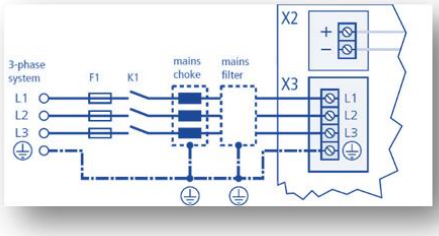

Figure 14. Detail of control units' three-phase system control unit.

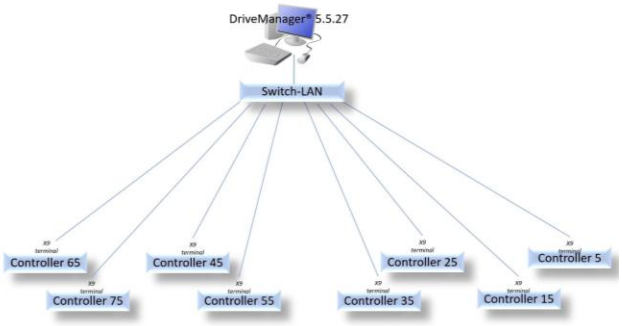

Figure 15. PC/ drive controllers' connection

After the correct mechanical installation and wiring with all required voltage supplies and external components, the software DriveManager® 5.5.27 was used to program and enable controlled movements of the system. Specific parameters were set by way of the command dialog box, Fig. 16.

In detail, motor data and control were manually set into "Motor identification" dialog box (Figure 16, on the top); the motors' phase check for monitoring the motors wiring was then achieved.

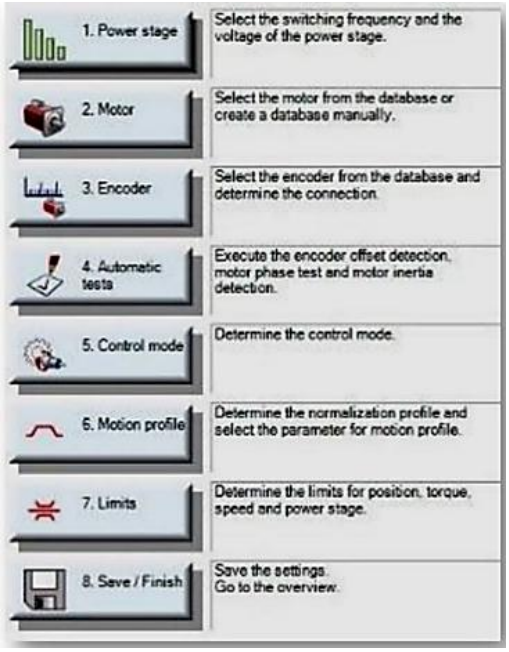

Figure 16. DriveManager® 5.5.27 dialog box for controllers and motors programming

Each motor can be schematized as an electrical "box", as shown in Fig.17: input signals are provided by means of X1. a terminal, while the output ones are channelled in X6 plug.

Moreover, since the power stages of controllers can be operated with different voltages and switching frequencies, the voltage and the switching frequency was adapted to the conditions corresponding to the investigated multi-axis system, as depicted in Figure 16 (on the right bottom corner). A maximum voltage reference value equal to 230 V was set for power failure bridging in closed-loop controlled mode; in such a way, if the voltage fell below 95% of that value, the motors speed would run down to zero fastest possible, according to a pre-set quick-stop ramp.

For evaluation of the resolver, X6 programming was achieved by means of 6 pins, as explicated in Fig. 18.

The current positional information was transmitted from the encoder to the receiver by means of X8 slot.

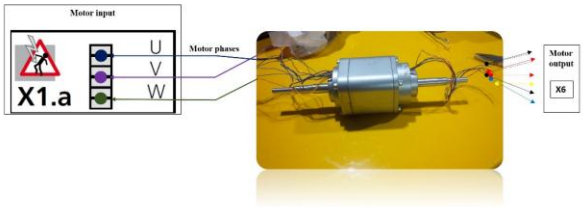

Figure 17. Motor input and output plugs schematization.

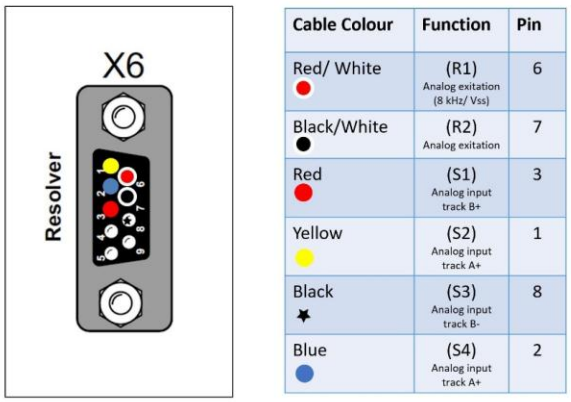

Cable Colour	Function	Pin
Red/ White	(R1) Analog exitation (8 kHz/ Vss)	6
Black/White	(R2) Analog exitation	7
Red	(S1) Analog input track B+	3
Yellow	(S2) Analog input track A+	1
Black	(S3) Analog input track B-	8
Blue	(S4) Analog input track A+	2

Figure 18. X6 resolver pin assignment.

More in detail, encoder interface X8 enables evaluation of several encoder types, depending on the specific application. In this activity, TTL encoder with zero pulse was considered and programmed with the pins set out in Fig. 19. The TTL module can simulate a TTL encoder with the aid of encoder simulation: this function forms incremental encoder-compatible pulses from the position of the rotary encoder connected to the motor. Two 90 °offset signals are generated on tracks A and B as well as a zero pulse (track R), Fig. 19.

In general, inaccuracy of the measuring system, slack in mechanical elements and thermal expansion of mechanical components may cause a significant difference between the actual position value delivered by the encoder system and the real position value on the axis. For this reason, such non-linear inaccuracies were properly compensated by axis error correction, by using position- and direction- dependent correction values.

Based on these considerations, the most suitable control system configuration for the flap required movements was elaborated (Fig. 20).

		Master controller	Slave controllers
Connection	X8 pin no.	Assignment TTL encoder	Assignment TTL encoder simulation
Female	1	A-	-
	2	A+	-
	3	+5 V (+/-) 5%, Imax = 250 mA loop-controlled	-
	4	-	A+
	5	-	A-
	6	B -	-
	7	-	R+ (zero pulse)
	8	+5 V	-
	9	R- (zero pulse)	-
	10	R+ (zero pulse)	-
	11	B+	-
	12	-	R- (zero pulse)
	13	-	GND
	14	-	B+
	15	-	B -

Figure 19. TTL encoder X8 slot pin assignment.

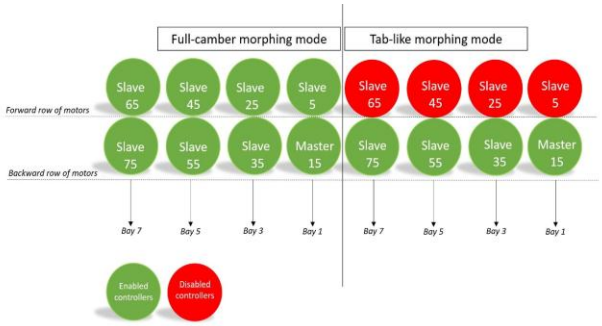

Figure 20. Control logic for bi-modal morphing mode activation.

Aiming to implement the two control laws, the followed steps were:

1. Homing procedure: for both the forward and the backward row of motors, a manual mechanical alignment of the motors' axes was carried out (morphing flap baseline configuration). Such a position was then assumed as absolute zero point for which activate the axes rotations, according with the target morphed shapes.

2. Electronic gear settings: this phase was mandatory to enable synchronized motion of the slave motors with respect to the master one. The gear ratio was assigned in fractions to ensure that the (homing) reference position could be translated to the motor shaft with no rounding error. Details about the given values are summarized in Figures 21 and 22.

3. Master configuration: speed, acceleration and deceleration were set, according with the point 2.

4. Synchronization mode: motors position control was performed by implementing each morphing mode in a tabular way into the master controller, while the slave control units served the master command (point 2). Reference table columns were indexed by numbers 0, 1 for the camber morphing and by 0, 1, 2, 3 for the tip down and up deflections. More in detail, the index:

• 0 corresponded to anticlockwise rotation of each motor's axis, from the baseline to the morphed-down configuration (both modes 1 and 2);

• 1 corresponded to clockwise rotation of each motor's axis, from the morphed-down to the baseline shape (both modes 1 and 2);

• 2 corresponded to clockwise rotation of the forward row of motors' axes, from the baseline to the morphed-up configuration (mode 2);

• 3 corresponded to anticlockwise rotation of the forward row of motors' axes from the morphed-up to the baseline configuration (mode 2).

The delay time between two consecutive positions was arbitrarily set equal to 5 seconds. Figure 23 shows the dialog box for the tabular control laws ([15]), while in Figures 24 and 25 the parameters set are depicted.

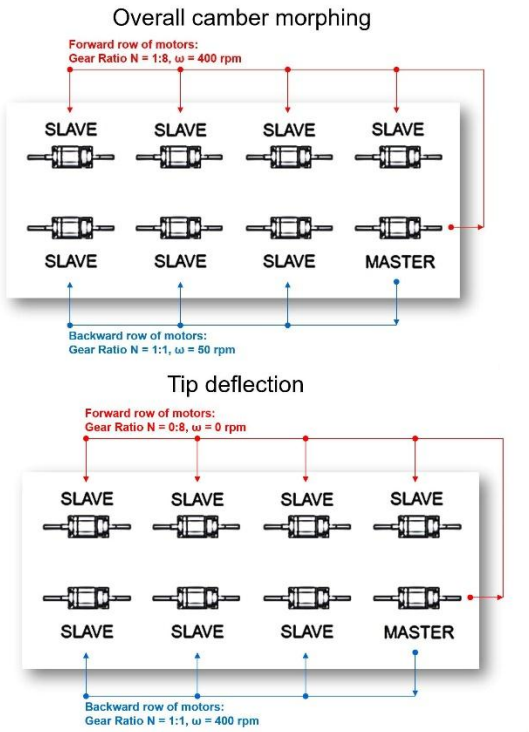

Figure 21. Electronic gear transmission ratio for morphing mode 1 (on the top) and 2 (on the bottom).

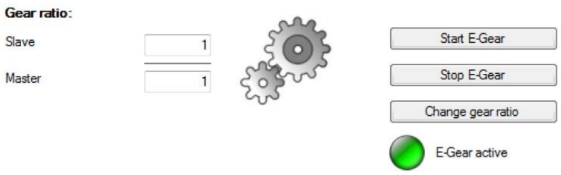

Figure 22. Slave/Master gear ratio command window ([15])

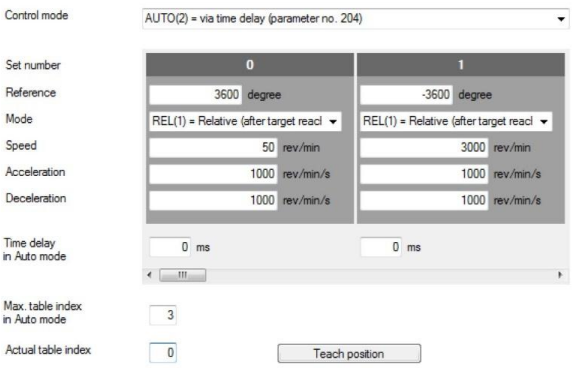

Figure 23. Dialog box for control mode ([15])

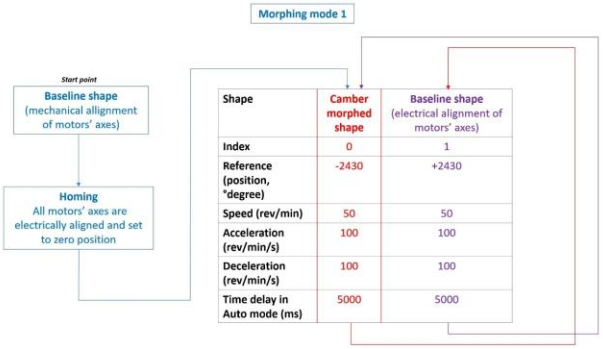

Figure 24. Control law set to enable the flap camber morphing

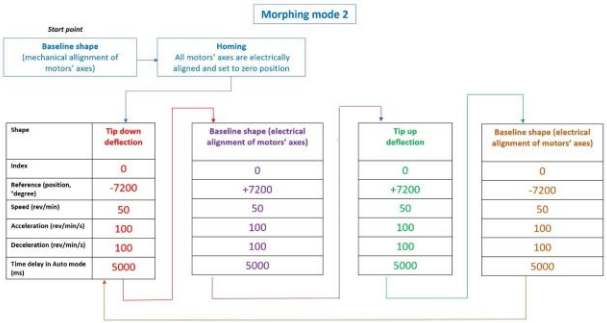

Figure 25. Control law set to enable the flap tab-like morphing

C. Sensing System Definition

To detect relative rotations between the blocks of two consecutive ribs, proper sensing instrumentation was chosen and installed inside the morphing flap for both actuators and controllers. More specifically, incremental encoders (IG04M, Siko® GmbH, Figure 19 [16]) were keyed to cylindrical hinges of ribs (A, B, C; Figure 4) placed along the span at the first, the third and the eighth stations from the root to the tip of the flap. Table 3 reports the technical data of the encoders [16].

Figure 26. IG04M, Siko® GmbH incremental encoder sensors, a), and display units, b) zoom.

TABLE III. TECHNICAL DATA OF ENCODER

Encoder Model	IG04M, Siko® GmbH
Operating Voltage	10 up to 30 VDC
Power input	250 mW (without load)
Geometrical Size	Through hollow shaft up to a maximum diameter of 14 mm with plain or ball bearing
Encoder Model	IG04M, Siko® GmbH
Material	Housing made of reinforced plastic

Each encoder was linked to its own display unit (MA55-0001, Siko ®; Figure 20) and required a power supply of 24 VDC ±20%.

IV. FUNCTIONALITY TEST

Functionality tests were carried out to validate the flap morphing capabilities [17]. The open loop law presented in Table 4 was implemented in a DriveManager® software environment to exploit the ability of the control devices to respond to a digital logic with various inputs by the X4 terminal (Figure 21). Each X4 terminal digital channel was specifically programmed to keep in memory a command to be executed when required by a board of five switches. For the ISD01 and ISD02 channels, the input speed (400 rpm) and the acceleration and deceleration values (100 rpm/s) were the same, but the following were different:

- Motor axis reference position (Figures 16 and 17), which was [0°, +10°] for the camber (to obtain hinge rotations of $\alpha A = 3°$, $\alpha B = 11°$, and $\alpha C = 3°$), and [−0°, +10°] for the tab-like deflection;
- Gear ratio (N) between the slave and master devices was set to 1:8 and 1:1 for the first and second rows of motors respectively, in the chord-wise direction.

The relative rotation between rib segments was measured with encoders corresponding to the hinges between consecutive blocks, as described in Section 3. These sensors made it possible to monitor the achieved morphed shapes and check for their full compliance with the design values [18].

Figures 27 shows the achieved morphed shapes during the functionality tests. The correlation level with the target configurations was judged to be more than satisfactory [19, 20].

TABLE IV. LOGIC CONTROL LAWS IMPLEMENTED IN THE X4 CONTROLLERS' TERMINAL

Digital channel Programmed	Camber morphing activation	Tip up and down Deflection. activation
ISD00: switching on for all controllers	On	On
ISD01: camber morphing start	On	Off
ISD02: tip deflection start	Off	On
ISDSH: safe standstill	On	On
ENPO: enable power	On	On

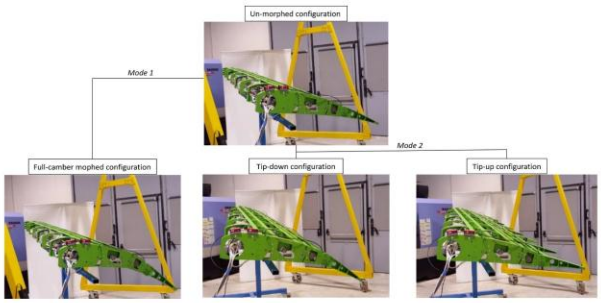

Figure 27. Bi-modal flap morphing configurations activated during the functionality test.

V. CONCLUSIONS

A novel true-scale morphing flap is presented. This paper particularly focused on the actuation and control system, which was analysed and designed to assure overall device compliance with industrial standards and applicable airworthiness requirements. The actuation is performed by a multi-axis system with eight hollow shaft brushless motors and eight controllers (one for each motor) for motion control. By exploiting the controllers' capability of acting as a master or slave, two proper digital control laws were implemented so that the motors could rotate by a specific gear ratio to reach the two target morphed shapes of the flap: overall camber morphing and tip deflections. The use of encoder sensors to measure the rotations of the rib blocks ensures that the morphed shapes were monitored, verifying their full correspondence with the target shapes. Undoubtedly, the idea herein described leads the way to further researches aimed at enhancing the TRL of the concept. To this aim, some remarks should be done on the most critical aspects of the current device. In particular, a future step may be the realization of a closed-loop control system. In such a way, flap motion measure and control could accurately occur by monitoring its output and "feeding" some of it back to compare the actual output with the desired one. This could make possible to reduce the error and, if disturbed, bring the output of the system back to the original or desired response, always ensuring the compliance with the target shapes of the flap.

REFERENCES

[1] R. Pecora, F. Amoroso, M. Magnifico, I. Dimino, and A. Concilio, "KRISTINA: Kinematic rib based structural system for innovative adaptive trailing edge," in *Proc. the SPIE Smart Structures/NDE Conference*, Las Vegas, NV, 2016.

[2] R. Pecora, A. Concilio, I. Dimino, F. Amoroso, and M. Ciminello, "Structural design of an adaptive wing trailing edge for enhanced cruise performances", in *Proc. the 24th AIAA/AHS Adaptive Structures Conference, AIAA SciTech*, San Diego, CA, 2016.

[3] Pecora, R., Barbarino, S. Concilio, A. Lecce, L., and Russo, S., "Design and functional test of a morphing high-lift device for a regional aircraft," *Journal of Intelligent Material Systems and Structures*, vol. 22, No. 10, pp. 1005–1023, 2011.

[4] Clean Sky, The Greening of Aviation, 2016. Available at: http://www.cleansky.eu

[5] R. Pecora, F. Amoroso, and M. Magnifico, "Toward the bi-modal camber morphing of large aircraft wing flaps: The CleanSky experience", in *Proc. the SPIE Smart Structures/NDE Conference*, Las Vegas, NV, 2016.

[6] M.C. Noviello, F. Rea, M. Arena, R. Pecora, and F. Amoroso, "Actuation and control of a novel wing flap architecture with bi-modal camber morphing capabilities," in Proc. of *the ICMAE Conference*, London, UK, 2016.

[7] F. Rea, M. Arena, M.C. Noviello, R. Pecora, and F. Amoroso, "Preliminary failure analysis of an innovative morphing flap tailored for large civil aircraft applications," in *Proc. the ICMAE Conference*, London, UK, 2016.

[8] R. Pecora, M. Magnifico, F. Amoroso, L. Lecce, M. Bellucci, I. Dimino, A. Conciclio, and M. Ciminello, *SARISTU – Smart Intelligent Aircraft Structures*, Springer International Publishing, Cham (ZG), Switzerland, 2016.

[9] Pecora, R., Amoroso, F., and Lecce, L., "Effectiveness of Wing Twist Morphing in Roll Control," *Journal of Aircraft*, vol. 49, no. 6, pp. 1666-1674, 2012.

[10] S. Barbarino, O. Bilgen, R. M. Ajaj, M. I. Friswell, and D. J. Inman, "A review of morphing aircraft," *Journal of Intelligent Material Systems and Structures*, vol. 22, pp. 823–877, 2011.

[11] S. Barbarino, R. Pecora, L. Lecce, A. Concilio, S. Ameduri, , and L. De Rosa, "Airfoil structural morphing based on S.M.A. actuator series: Numerical and experimental results," *Journal of Intelligent Material Systems and Structures*, vol. 22, pp. 987–1004, 2011.

[12] E. Stanewsky, "Adaptive wing and flow control technology," *Progress in Aerospace Sciences*, vol. 37, no. 7, pp. 583–667, 2001.

[13] G. Amendola, I. Dimino, A. Concilio, R. Pecora, and F. Amoroso, *Morphing Wing Technologies: Large Commercial Aircraft and Civil Helicopters*, Elsevier Butterworth-Heinemann, Oxford, UK, 2017.

[14] R. Pecora, S. Barbarino, A. Concilio, L. Lecce, and S. Russo, "Design and functional test of a morphing high-lift device for a regional aircraft," *Journal of Intelligent Material Systems and Structures*, vol. 22, pp. 1005–1023, 2011.

[15] LTI Motion, Manufacturer of industrial automation systems, 2016. Available at: http://www.lti-motion.com.

[16] Siko-Global, Measure sensors and instruments, 2016. Available at: https://www.siko-global.com/it-it.

[17] R. Pecora, F. Amoroso, M. Arena, M. C. Noviello, and F. Rea, "Experimental validation of a true-scale flap for large civil aircraft applications", in *Proc. the SPIE Smart Structures/NDE Conference*, Portland, OR, 2017.

[18] G. Amendola, I. Dimino, A. Concilio, F. Amoroso, R. Pecora, "Preliminary design of an adaptive aileron for the next generation

regional aircraft," *Journal of Theoretical and Applied Mechanics*, vol. 55, no. 1, pp. 307–316, 2017.
[19] European Aviation Safety Agency, Certification Specifications and Acceptable Means of Compliance for Large Aeroplanes – CS-25, Amendment 11, July 2011.
[20] S. Barbarino, O. Bilgen, R. M. Ajaj, M. I. Friswell, and D. J. Inman, "A review of morphing aircraft," *Journal of Intelligent Material Systems and Structures*, vol. 22, 2011, pp. 823-877.

M. C. Noviello was born in Cerreto Sannita (BN) (Italy), on January, the 6th 1991. She graduated with honors in Aerospace Engineering at the University of Naples "Federico II" with a master's thesis about the experimental shape reconstruction of a morphing wing trailing edge prototype, achieved on April, the 7th 2015. She is currently a Ph. D. Candidate in Industrial Engineering. In her research, she investigates aeroelastic trade-off analyses of adaptive trailing edge devices for wing load control. Other activities regard the control system design for a morphing wing flap demonstrator. She is author of seven scientific papers presented at conferences or published into specialized journals.

F. Rea has a master's degree in Aerospace Engineering at University of Naples "Federico II". He is an Industrial Engineering Ph.D. Candidate; he is employed in several adaptive structures projects, dealing with the design, finite element modelling and analyzing, experimental tests.

M. Arena has a master's degree in Aerospace Engineering at University of Naples "Federico II". He is currently an Industrial Engineering Ph.D. Candidate. His field of research is centred on advanced aerospace structures, from their design to experimental validating and testing process.

R. Pecora is responsible of the course "Stability of Aircraft Structures" at University of Naples "Federico II". He is honorary fellow in the following disciplines:
-Aircraft Structures;
-Aeroelasticity.
Head of Smart Structures Laboratory. Team leader of several research projects focused on innovative aircraft structures.

F. Amoroso is researcher in Aircraft Structures at University of Naples "Federico II". He teaches "General Design of Turbomachines". He is specialized in design, modelling, analyses and overall development of advanced aircraft components.